kinases and phosphatases

MDPI

Article

Targeting the Activation Segment with Peptidomimetics: A Computational Strategy for Selective Kinase Inhibition

Adil Ahiri [1,*] and Aziz Aboulmouhajir [2]

[1] Modeling and Molecular Spectroscopy Team, Faculty of Sciences, Chouaib Doukkali University, El-Jadida 24000, Morocco
[2] Laboratory of Materials, Process and Environmental Engineering, Team of Treatment, Valorization and Mechanisms, Faculty of Sciences Ain Chock, Hassan II University, Casablanca 20470, Morocco
* Correspondence: ahiri.adil@gmail.com

Abstract

Protein kinase inhibition can be achieved through various mechanisms, including blocking phosphorylation activity or disrupting regulatory interactions. While small molecule inhibitors have shown promise, their selectivity remains challenging due to the structural similarities among kinase catalytic sites. To design selective kinase inhibitors based on peptide terminal tail interactions with the activation segment, focusing on five kinases with different conformational states: GSK3, PAK4, TTN (OUT conformation) and PKB, FLT3 (IN conformation). Three-dimensional structures from RCSB PDB were optimized using MODELLER version 9.0. Peptide sequences were designed with PeptiDerive (Rosetta) and RosettaDesign version 3.5, followed by pharmacophore modeling based on key interaction residues. Virtual screening was then conducted with PyRx 0.8 and molecular docking with AutoDock Vina 1.1.2. Molecular dynamics simulations were performed using Desmond v6.6 (Schrödinger Suite 2016, Multisim v3.8.5.19) (100 ns, NPT ensemble, 300 K). Analysis of the five kinases revealed distinct interaction profiles with designed peptidomimetic compounds. Kinases displaying the IN conformation of the activation segment (PKB and FLT3) consistently showed superior stability and stronger interaction profiles compared to those in the OUT conformation. The designed compounds formed key hydrogen bonds and hydrophobic interactions with critical residues in the activation segment binding pocket. The most promising inhibitors demonstrated stability throughout the molecular dynamics simulations, with IN conformation kinases maintaining more consistent conformational profiles than their OUT conformation counterparts. Kinases with IN conformation of the activation segment demonstrated superior stability and interaction profiles compared to OUT conformations. These findings contribute to our understanding of selective kinase inhibition and provide a framework for developing novel inhibitors, particularly for PKB and FLT3. The implications of this study extend to rational drug design approaches that leverage natural regulatory mechanisms for therapeutic intervention, though further optimization is needed for GSK-3β, PAK4, and TTN to improve stability and binding affinity.

Keywords: kinase inhibitors; activation segment; peptidomimetics; protein–peptide interactions; molecular docking; molecular dynamics simulation; terminal tail regulation

Check for updates

Academic Editor: Mauro Salvi

Received: 19 January 2026
Revised: 28 February 2026
Accepted: 19 March 2026
Published: 26 March 2026

Copyright: © 2026 by the authors. Licensee MDPI, Basel, Switzerland. This article is an open access article distributed under the terms and conditions of the Creative Commons Attribution (CC BY) license.

1. Introduction

Protein kinases play a vital role in cellular signal transduction and represent significant targets for therapeutic intervention. The inhibition of kinase protein activity can be achieved

through various mechanisms, including blocking phosphorylation activity or disrupting regulatory interactions. Over the past decade, small-molecule kinase inhibitors have been the subject of intensive research, primarily as novel anticancer therapies [1]. However, the selectivity of these small molecules remains challenging for protein kinases that share similar three-dimensional structures of the catalytic site [2,3].

Recent advances in peptide-based therapeutics have opened new possibilities for targeting protein kinases. Peptides offer several advantages over small molecules, including higher specificity and potentially reduced toxicity [4,5]. This advantage stems from several physicochemical properties: Peptides provide larger interaction surfaces, enabling recognition of extended binding sites beyond the ATP pocket, with substrate-binding sites comprising up to 32 residues compared to the limited contacts made by ATP [6], can effectively target protein–protein interaction interfaces that are challenging for small molecules [7], and achieve sequence-specific recognition through multiple contacts that reduce off-target binding [8]. Furthermore, natural proteolytic degradation of peptides limits accumulation and prolonged off-target effects.

The success of peptide-based drugs in other therapeutic areas suggests untapped potential in kinase inhibition [9].

Therefore, the use of peptides may prove advantageous as they can more faithfully mimic binding modes within the kinase active site. Furthermore, the high specificity and low toxicity of peptide drugs stem from their extremely tight binding to their targets [4]. This highlights the importance of leveraging known protein–peptide complex structures [10,11]. At protein–peptide interaction surfaces, a limited number of "hot spot" residues play a crucial role in binding, with binding affinity being considerably reduced when these are mutated to alanine [12,13]. Consequently, understanding the location and binding mode of these hotspots can provide an optimal pathway for rational drug design [14].

Several classes of peptide inhibitors are possible:

Class 1: The peptide inhibitor mimics the binding sites of a scaffold protein, which acts as an organizational platform hosting both the phosphorylating kinase and the phosphorylated substrate.

Class 2: The peptide inhibitor competes with the substrate at its binding sites, thereby preventing kinase–substrate interactions.

Class 3: The peptide inhibitor competes with the substrate at its recognition sites outside the active site. This class may also include pseudo-substrates, which are segments of polypeptide chains that occupy the kinase active site and lead to auto-inhibition. Indeed, auto-inhibition represents a common allosteric regulatory mechanism in kinases.

Among the structural elements controlling kinase activity, the activation segment (A-loop) serves as a central regulatory switch that adopts distinct conformations to control substrate access and catalytic function [15,16]. The A-loop can adopt an active "OUT" conformation, in which it extends away from the catalytic cleft to allow substrate binding, or an inactive "IN" conformation, in which it folds into the active site and blocks catalysis [15]. Importantly, many kinases possess regulatory terminal tails—including N-terminal extensions, C-terminal tails, juxtamembrane segments, and pseudosubstrate domains—that directly interact with the activation segment to stabilize these conformational states and auto-inhibit kinase activity [17,18]. For example, the pleckstrin homology (PH) domain of PKB anchors within the groove formed by the IN-folded activation segment [19,20], the juxtamembrane segment of FLT3 stabilizes the inactive conformation through contacts with the A-loop [18], and the pseudosubstrate domain of PAK4 occupies the substrate-binding site adjacent to the activation segment [21]. These natural peptide–activation segment interactions represent attractive starting points for inhibitor design, as they exploit ex-

tended and kinase-specific binding surfaces that differ substantially from the conserved ATP-binding pocket.

Despite the importance of the activation segment (A-loop) in kinase regulation being well-documented [15,16], there remains a significant gap in our understanding of how peptide-based inhibition can specifically target this region. To date, no studies have systematically explored the relationship between activation segment conformation (IN/OUT) and inhibitor binding efficiency [22].

Given the availability of a series of auto-inhibited kinases, and considering the previously mentioned importance of the A-loop [15,23] (a regulatory phosphorylation zone with high specificity), we aimed to investigate its interaction with the inhibitor. Recent structural studies have revealed that many kinases possess terminal tails that regulate activity through interaction with the activation segment [17,18]. This natural regulatory mechanism, combined with advances in computational methods for peptide design [24,25], creates a timely opportunity to explore novel inhibition strategies. The purpose was to identify residues with conserved positions and/or interactions, thereby developing a highly specific means of inhibiting kinases via their A-loop. To date, to our knowledge, no studies have investigated the possibility of designing computational mimetics of regulatory terminal tail interactions for kinase inhibition targeting the A-loop. In this study, we present a peptidomimetic design strategy that computationally mimics the key interactions between regulatory terminal tails and the activation segment. Our approach integrates peptide design (PeptiDerive (Rosetta), RosettaDesign version 3.5), pharmacophore modeling of critical peptide–kinase contacts (PIZSA (http://cospi.iiserpune.ac.in/pizsa/, accessed on 24 June 2020), PepMMsMIMIC (http://mms.dsfarm.unipd.it/pepMMsMIMIC/, accessed on 7 July 2022)), virtual screening against peptidomimetic libraries (MMsINC (http://mms.dsfarm.unipd.it/MMsINC/search/, accessed on 7 July 2022)/PyRx 0.8), molecular docking (AutoDock Vina 1.1.2), and molecular dynamics validation (Desmond v6.6, Schrödinger Suite 2016, Multisim v3.8.5.19). We apply this workflow to five kinases spanning distinct families—GSK-3β, PAK4, and TTN (OUT conformation) and PKB and FLT3 (IN conformation)—to: (1) identify small molecules that reproduce the essential interactions of regulatory tail peptides with the activation segment, (2) evaluate whether the IN or OUT conformation of the activation segment preferentially supports stable peptidomimetic binding, and (3) establish a generalizable computational framework for activation segment-targeted kinase inhibitor discovery.

2. Results

We applied the computational workflow described in Materials and Methods (Figure 1) to five kinase targets representing distinct structural families. For each kinase, we report the screening metrics, top-ranked hits, and molecular dynamics stability analysis.

Five kinases were identified for this study: GSK3, PAK4, TTN, PKB and FLT3. As shown in Figure 1, these kinases are distributed across different groups, namely AGC, CAMK, CMGC, STE and TK, all of which possess terminal tails that regulate activity through interaction with the activation segment (Figure 1).

The OUT conformation of the activation segment, observed primarily in three kinases (GSK-3β, PAK4, TTN), allows effective substrate binding, with the A-loop in the OUT position and the P + 1 segment well-exposed adjacent to the ATP binding site (Figure 2a).

In contrast, the IN conformation of the activation segment, found predominantly in two kinases (PKB, FLT3), prevents substrate binding as the activation segment is folded into the ATP binding site (Figure 2b).

These two conformations provide a foundation for regulatory terminal tail binding, with kinase inhibition occurring through several mechanisms:

Terminal tail binding to the substrate binding site (pseudo-substrate)

Terminal tail binding to the ATP binding site

Terminal tail binding to the RD zone where the phosphorylated amino acid of the A-loop binds, rendering the activation segment inactive and thereby inhibiting kinase activity

It is important to note that the IN conformation of the activation loop enables access to interactions involving its β6-β9 sheets or even the entire A-loop pocket.

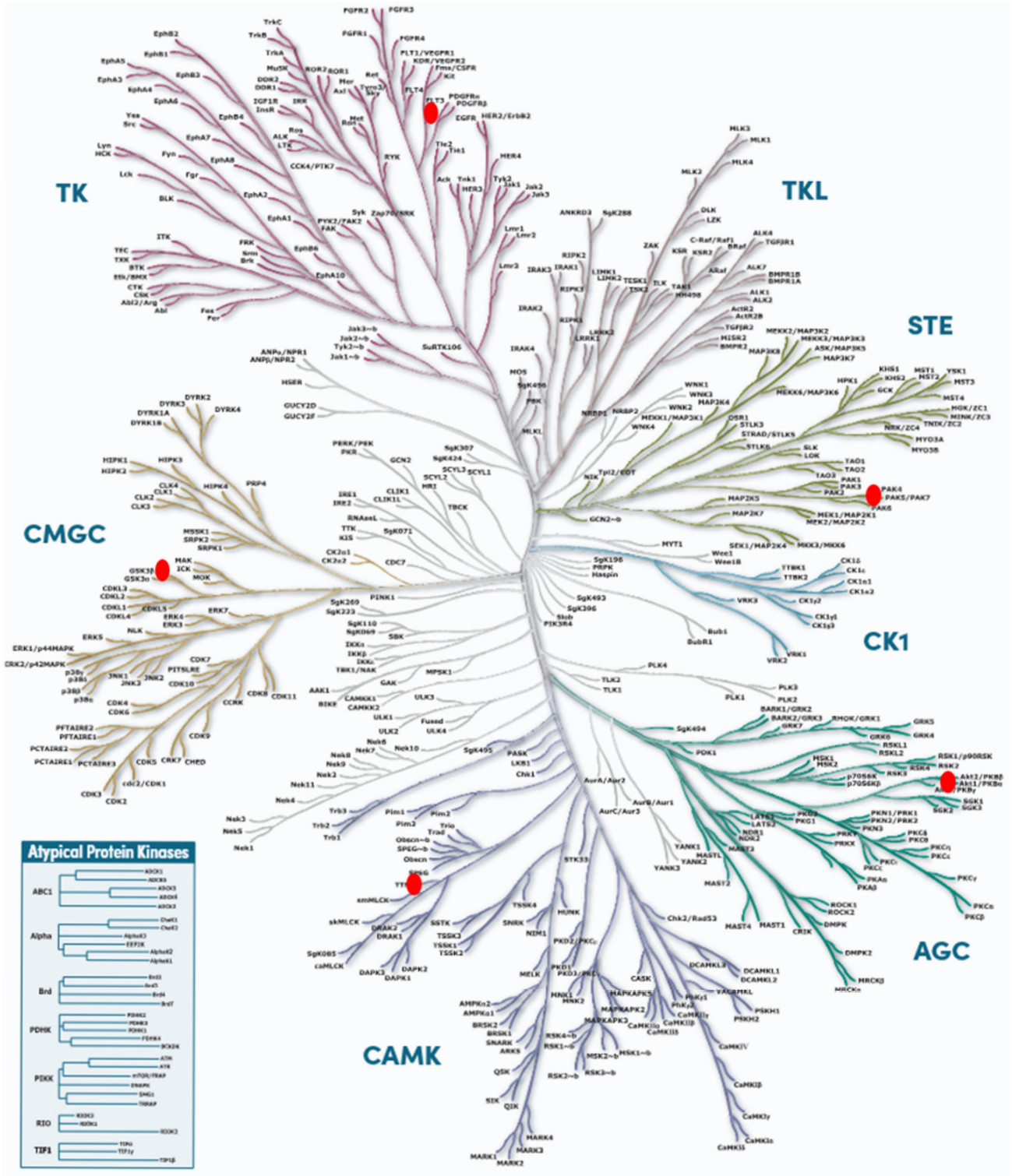


Figure 1. Phylogenetic tree of human ePK-type protein kinases. Kinases marked in red possess terminal tails responsible for regulation in the activation segment.

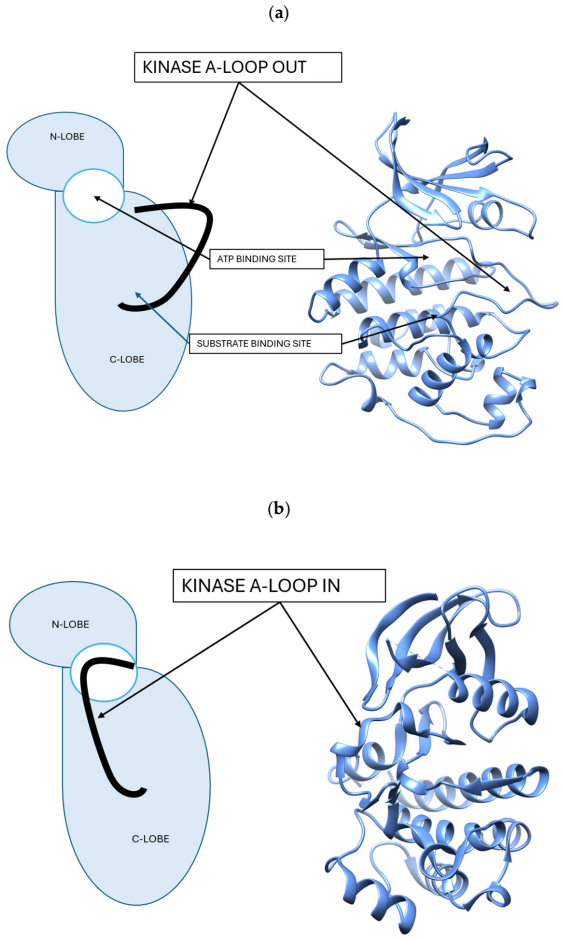


Figure 2. Visualization of the catalytic domain showing (**a**) the active conformation of the activation segment (OUT) and (**b**) the inactive conformation of the activation segment (IN).

2.1. PKB Kinase

PKB (PDB:6HHG-A, IN conformation) features a PH domain that, in its auto-inhibited state (PH IN), anchors between the two lobes of the catalytic domain and occupies the groove formed by the IN-folded activation segment (Figure 3). We targeted this PH domain–activation segment interface for inhibitor design. Using PeptiDerive (Rosetta), a ten-amino acid peptide (GEYIKTWRPR) from the PH domain was identified as having the highest interaction score with the A-loop (Figure 4).

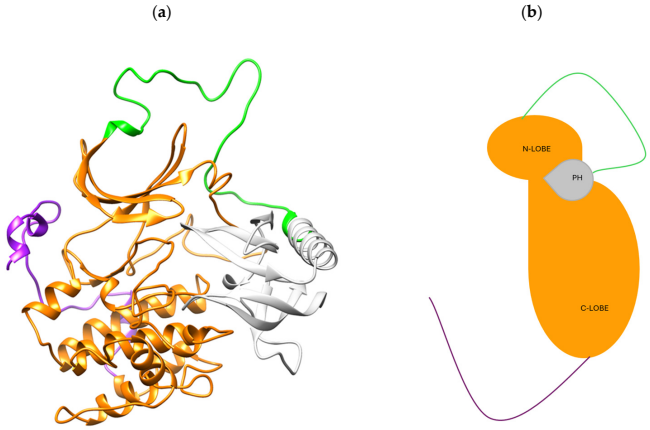


Figure 3. (**a**) X-ray crystal structure of the PKB kinase (orange), with the PH domain highlighted in gray. (**b**) Schematic representation of the PKB kinase. In (**a**,**b**), orange represents the kinase catalytic domain, gray highlights the PH domain, and green indicates the N-lobe.

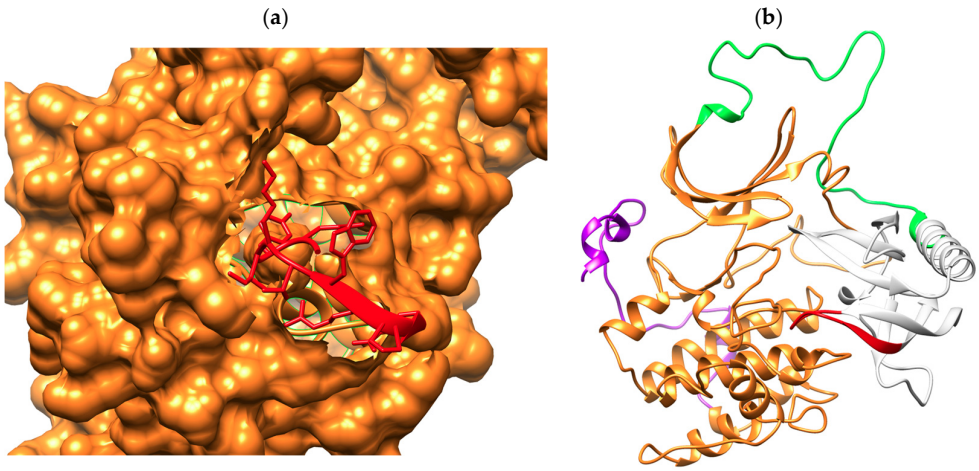


Figure 4. (**a**) Location of the ten–amino acid peptide (GEYIKTWRPR) from the PH domain (in red) on the PKB kinase surface (orange); (**b**) Three-dimensional molecular structure visualization of this peptide (in red) in relation to the PKB kinase (orange).

Using Rosetta.design 3.5, an analysis of the peptide's affinity toward its receptor PKB—specifically at the A-loop—led us to conclude that no further improvement can be envisaged to enhance its binding affinity. By focusing on these 10 amino acids, the PIZSA (http://cospi.iiserpune.ac.in/pizsa/, accessed on 24 June 2020) software enabled us to identify three adjacent peptide residues (chain B, PH domain)—Thr305, Ala304, and Met306—as those contributing most significantly to the interaction with the kinase activation segment (chain A). A virtual screening via PyRx 0.8 allowed us to detect the compound MMs01663909, which is the most likely candidate to reproduce the essential interactions of these three peptide residues with the A-loop pocket of PKB (Figure 5a). Furthermore, docking studies identified that this hit engages in two hydrophobic interactions with kinase residues Phe309 and Leu316 (chain A) and forms two hydrogen bonds with Asp323 and Arg273 (chain A) (Figure 5b).

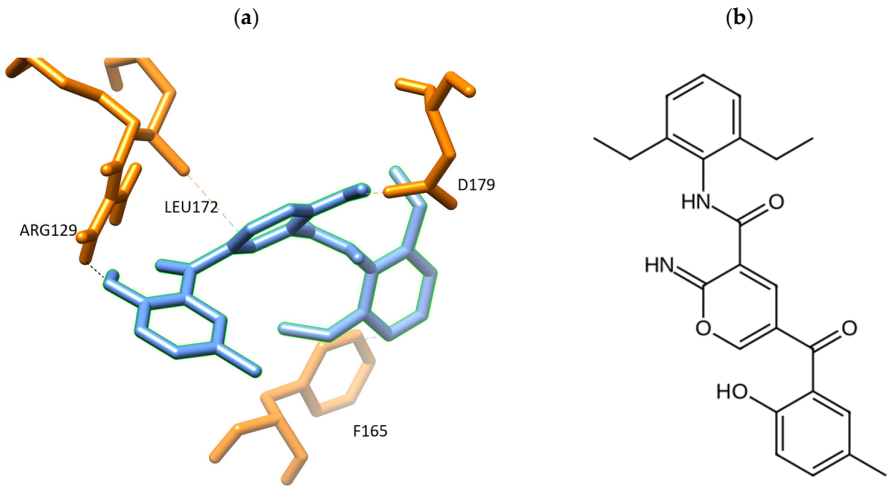


Figure 5. (**a**) Interactions involving the compound MMs01663909 within the PKB kinase following docking, orange sticks represent kinase residues and blue sticks represent compound; (**b**) the 2D compound MMs01663909 obtained after virtual screening.

Molecular dynamics simulations revealed ligand RMSD values stabilizing around 2.0 Å (Figure 6).

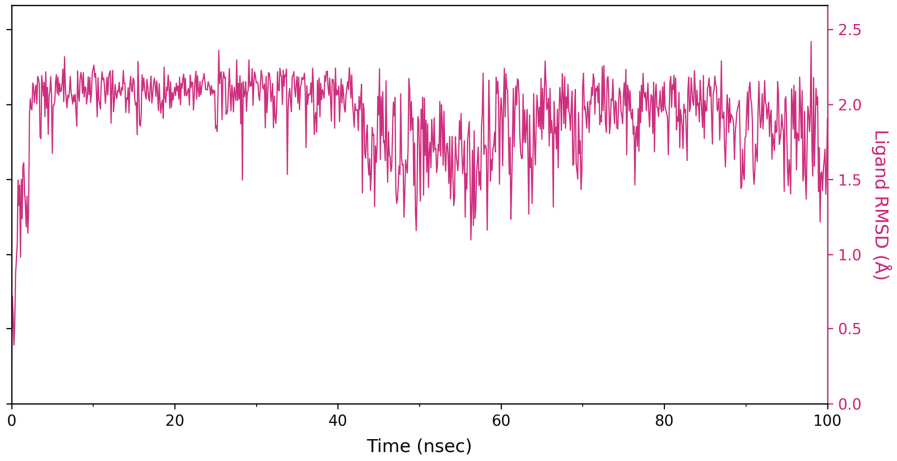


Figure 6. Molecular dynamics simulation (RMSD) of the interactions of MMs01663909 within the PKB kinase.

2.2. FLT3 Kinase

FLT3 (PDB:1RJB-A, IN conformation) is auto-inhibited through its juxtamembrane (JM) segment, which stabilizes the inactive kinase conformation (Figure 7). We targeted the JM segment–activation segment interface for inhibitor design (Figure 8).

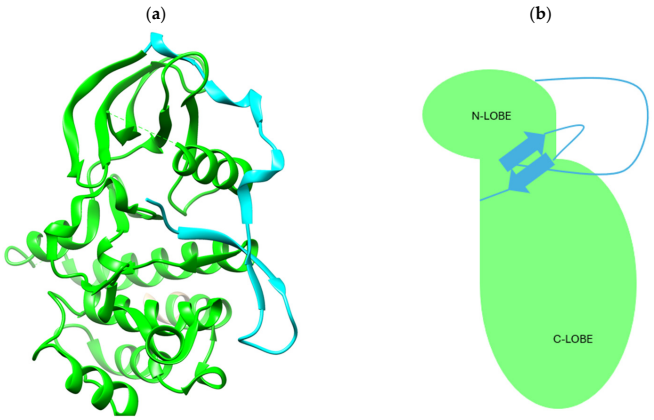


Figure 7. (**a**) X-ray crystal structure of the FLT3 kinase (green), with the C-terminal tail highlighted in cyan. (**b**) Schematic representation of the FLT3 kinase. In (**a**,**b**), green represents the FLT3 kinase, cyan highlights the C-terminal tail, and arrows indicate the beta sheet orientation of the juxtamembrane segment.

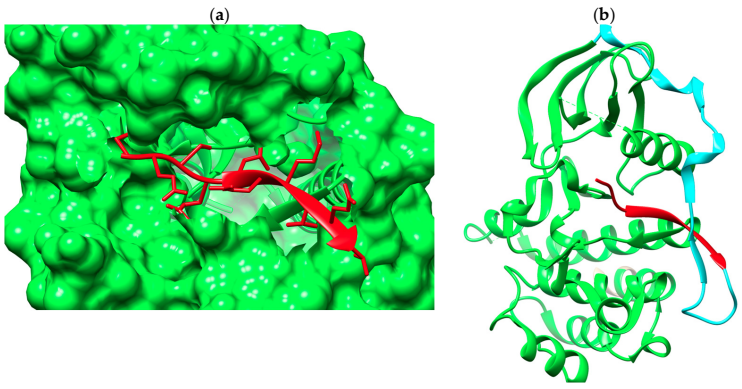


Figure 8. (**a**) Location of the ten-amino acid peptide (YESQLQMVQV) from the juxtamembrane segment (in red) on the FLT3 kinase surface (green); (**b**) Three-dimensional molecular structure visualization of this peptide (in red) in relation to the FLT3 kinase (green); cyan represents the JM segment.

Using PeptiDerive (Rosetta), we identified a ten–amino acid peptide (YESQLQMVQV) from the juxtamembrane segment that achieved the highest interaction score. To enhance this peptide's affinity for its FLT3 receptor, analysis with Rosetta.design 3.5 enabled us to introduce two modifications, namely Q274Y and V280F. The refinement of the complex's interaction was subsequently carried out using FlexPepDock (https://flexpepdock.furmanlab.cs.huji.ac.il/, accessed on 24 June 2020). Additionally, PIZSA (http://cospi.iiserpune.ac.in/pizsa/, accessed on 24 June 2020) allowed us to identify three adjacent peptide residues from the juxtamembrane segment (chain B) that contributed most significantly to this interaction: Leu275 (side chain, backbone CO, and backbone NH), Met277 (side chain, backbone CO, and backbone NH), and Val278 (side chain, backbone CO, and backbone NH). These peptide residues form key contacts with the kinase activation segment (chain A).

A virtual screening via PyRx 0.8 enabled us to detect the compound most likely to reproduce the essential interactions of these residues with the kinase (Figure 9a).

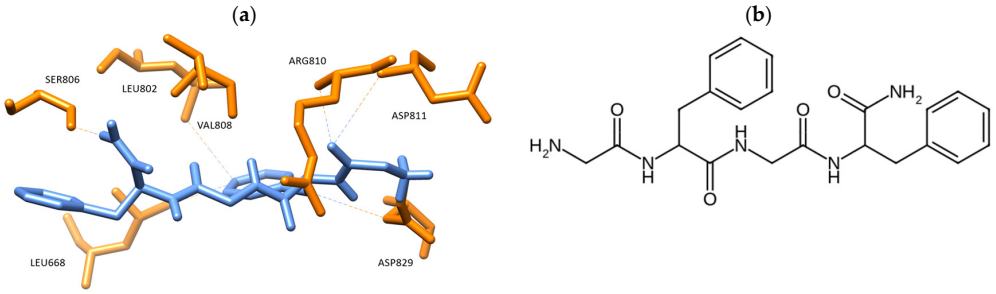


Figure 9. (**a**) Interactions involving the compound MMs02451714 within the FLT3 kinase following docking, orange sticks represent kinase residues and blue sticks represent compound; (**b**) the 2D compound MMs02451714 obtained after virtual screening.

Molecular docking allowed us to identify several hydrogen bonds with kinase residues (chain A) Asp811, Arg810, Val808, Leu802, Ser806, and Asp829, in addition to two hydrophobic interactions with Leu668 and Asp829 (chain A) (Figure 9b).

Molecular dynamics analysis revealed ligand RMSD values equilibrating between 1.5 and 2.0 Å (average 1.7–1.8 Å) (Figure 10).

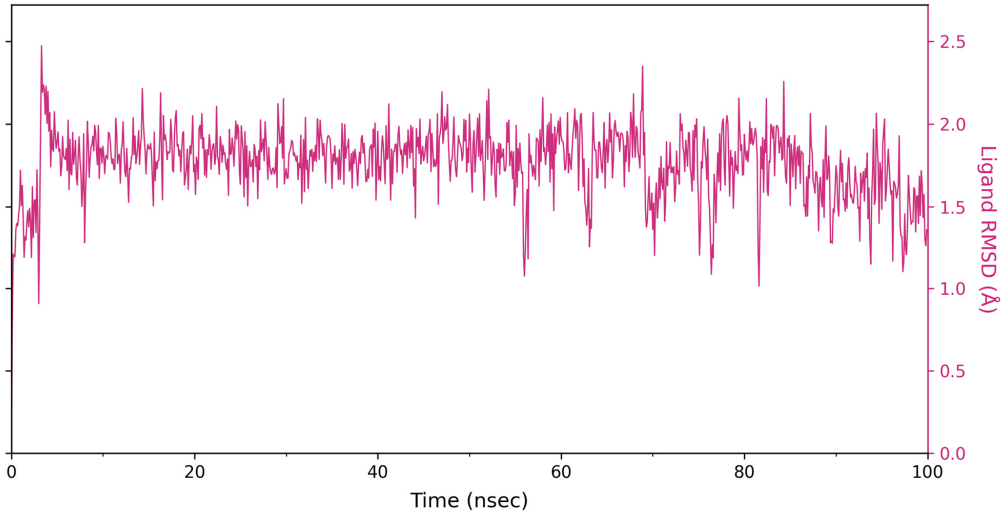


Figure 10. Molecular dynamics simulation (RMSD) of the interactions of MMs02451714 within the FLT3 kinase.

2.3. GSK-3β Kinase

GSK-3β (PDB:4NM3-A, OUT conformation) is auto-inhibited by the phosphorylated N-terminal pS9 peptide, which acts as a pseudosubstrate occupying the substrate-binding site (Figure 11).

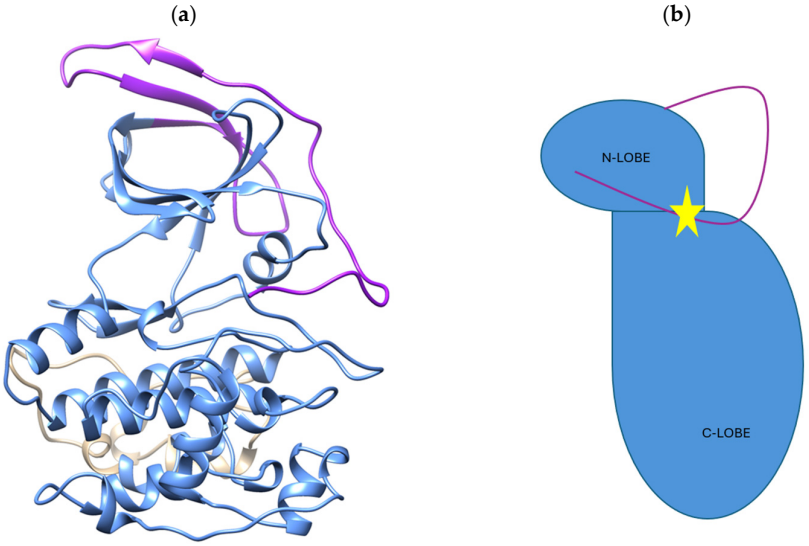


Figure 11. (**a**) X-ray crystal structure of the GSK-3β kinase (blue), with the N-terminal pseudosubstrate highlighted in violet. (**b**) Schematic representation of the GSK-3β kinase. In (**a**,**b**), blue represents the GSK-3β kinase, violet highlights the N-terminal pseudosubstrate, and the yellow star indicates the phosphorylation site (pS9).

We targeted the pS9 peptide–activation segment interface for inhibitor design (Figure 12).

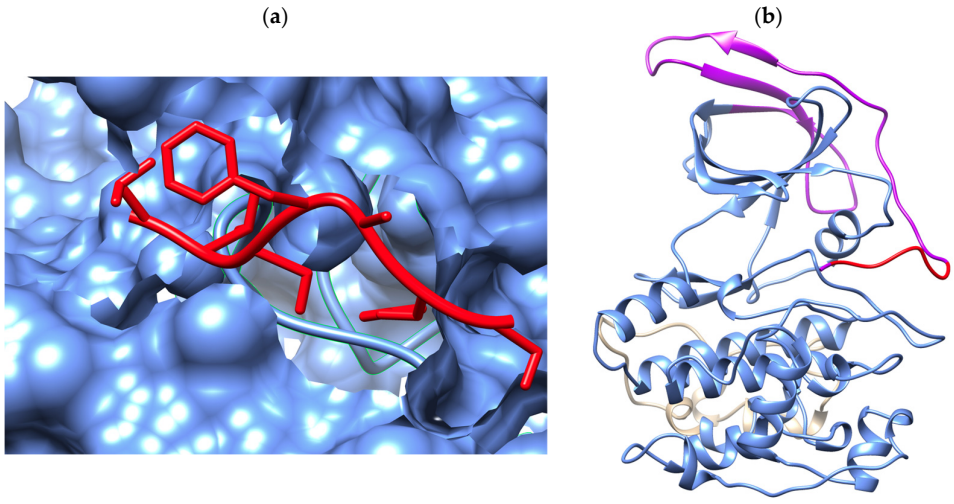


Figure 12. (**a**) Location of the seven-amino acid peptide (TTSFAES) from the N-terminal pS9 segment (in red) on the GSK-3β kinase surface (blue); (**b**) Three-dimensional molecular structure visualization of this peptide (in red) in relation to the GSK-3β kinase (blue); violet represents the N-terminal tail.

Through the application of PeptiDerive (Rosetta), this investigation identified a seven-amino acid peptide (TTSFAES) from this segment that exhibited the highest scoring profile. Subsequent analysis utilizing Rosetta.design 3.5 enabled the modification of one amino acid (S367Y) to enhance peptide affinity, followed by refinement procedures implemented through FlexPepDock (https://flexpepdock.furmanlab.cs.huji.ac.il/, accessed on 24 June 2020) [14].

Further analysis conducted via PIZSA (http://cospi.iiserpune.ac.in/pizsa/, accessed on 24 June 2020) revealed three peptide residues from the N-terminal pS9 segment (chain A) that made the most significant contributions to the interaction with the kinase catalytic domain: Phe4 (side chain), Ala5 (side chain), and Ser7 (side chain). These peptide interactions were subsequently mimicked through virtual screening using PyRx 0.8, resulting in the identification of compound MMs03699561 as the most likely candidate to represent these interactions with the kinase activation segment (Figure 13).

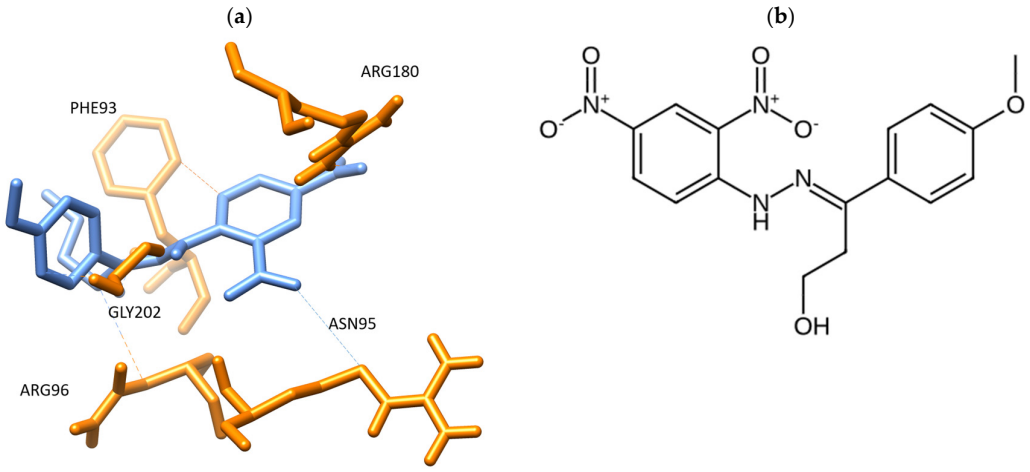


Figure 13. (**a**) Interactions involving the compound MMs03699561 within the GSK-3β kinase following docking, orange sticks represent kinase residues and blue sticks represent compound; (**b**) the 2D compound MMs03699561 obtained after virtual screening.

Molecular dynamics simulations revealed ligand RMSD values fluctuating between 1.2 and 2.1 Å (average 1.6 Å), with periodic oscillations (Figure 14).

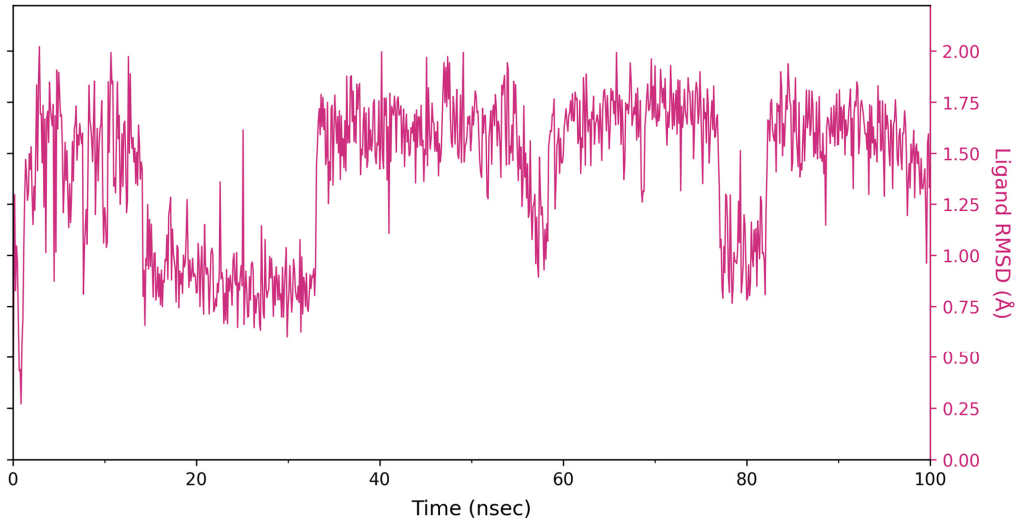


Figure 14. Molecular dynamics simulation (RMSD) of the interactions of MMs03699561 within the GSK-3β kinase.

2.4. PAK4 Kinase

PAK4 (PDB:4FIE-A, OUT conformation) is auto-inhibited by the pseudosubstrate domain (PSD), which occupies the substrate-binding site of the kinase (Figure 15). We targeted the PSD–activation segment interface for inhibitor design (Figure 16).

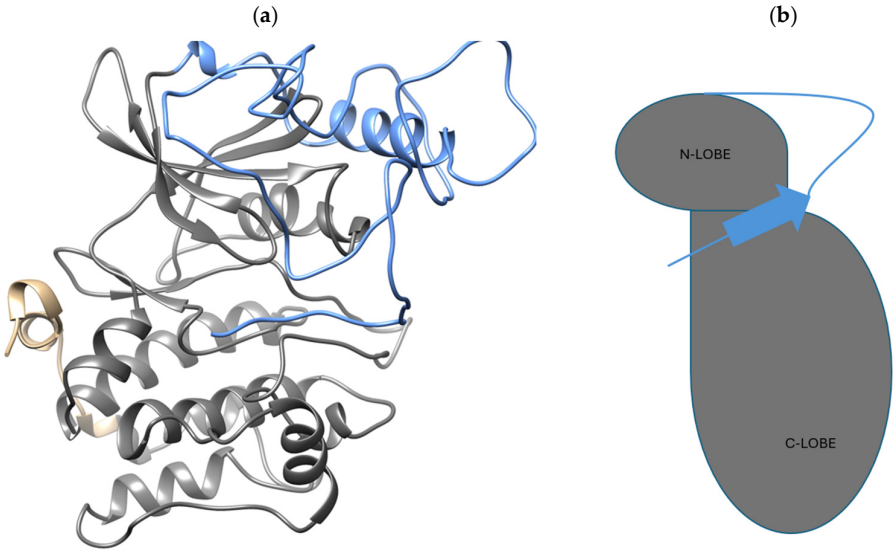


Figure 15. (**a**) X-ray crystal structure of the PAK4 kinase (gray), with the pseudosubstrate domain (PSD) highlighted in blue. (**b**) Schematic representation of the PAK4 kinase. In (**a**,**b**), gray represents the PAK4 kinase catalytic domain, blue highlights the pseudosubstrate domain (PSD), and arrows indicate the beta sheet orientation of the PSD.

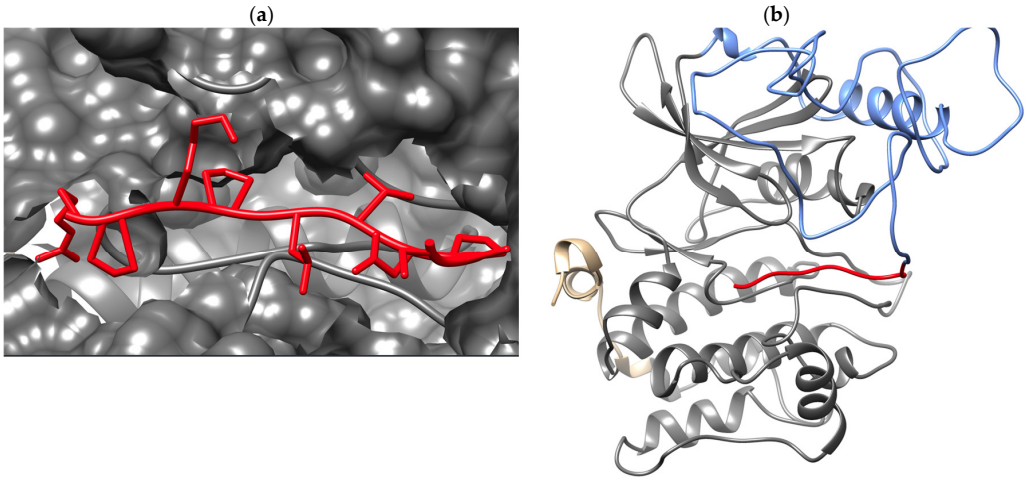


Figure 16. (**a**) Location of the ten-amino acid peptide (RPKPLVDPAC) from the pseudosubstrate domain (in red) on the PAK4 kinase surface (gray); (**b**) Three-dimensional molecular structure visualization of this peptide (in red) in relation to the PAK4 kinase (gray).

Through PeptiDerive (Rosetta) analysis, a ten-amino acid peptide (RPKPLVDPAC) from the pseudosubstrate domain was identified as exhibiting the highest scoring profile. Subsequent optimization attempts using Rosetta.design 3.5 to enhance the peptide's affinity towards its PAK4 receptor did not yield substantial improvements. PIZSA (http://cospi.iiserpune.ac.in/pizsa/, accessed on 24 June 2020) analysis facilitated the identification of three adjacent peptide residues from the pseudosubstrate domain (chain B) that demonstrated optimal interaction scores with the kinase catalytic domain (chain A): Pro298 (side chain), Ala299 (side chain), and Cys300 (side chain) (Figure 17).

Virtual screening implemented through PyRx 0.8 facilitated the identification of compound MMs03492885_c1 as the most promising candidate to mimic this triple residue interaction. Molecular docking analysis revealed two hydrogen bonding interactions with kinase residues (chain A) Gly447 and Lys442, complemented by a hydrophobic interaction with Phe461 (chain A). Molecular dynamics simulations revealed ligand RMSD values ranging from 1.5 to 2.4 Å (Figure 18).

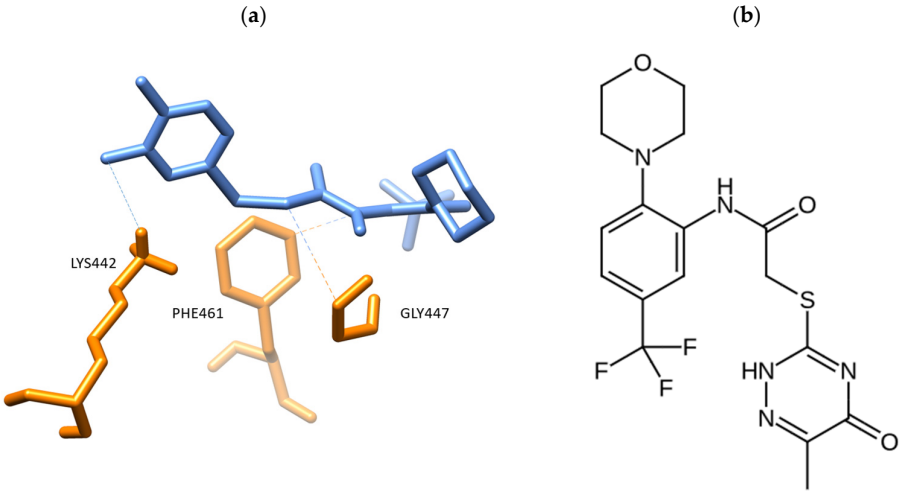


Figure 17. (**a**) Interactions involving the compound MMs03492885_c1 within the PAK4 kinase following docking, orange sticks represent kinase residues and blue sticks represent compound; (**b**) the 2D compound MMs03492885_c1 obtained after virtual screening.

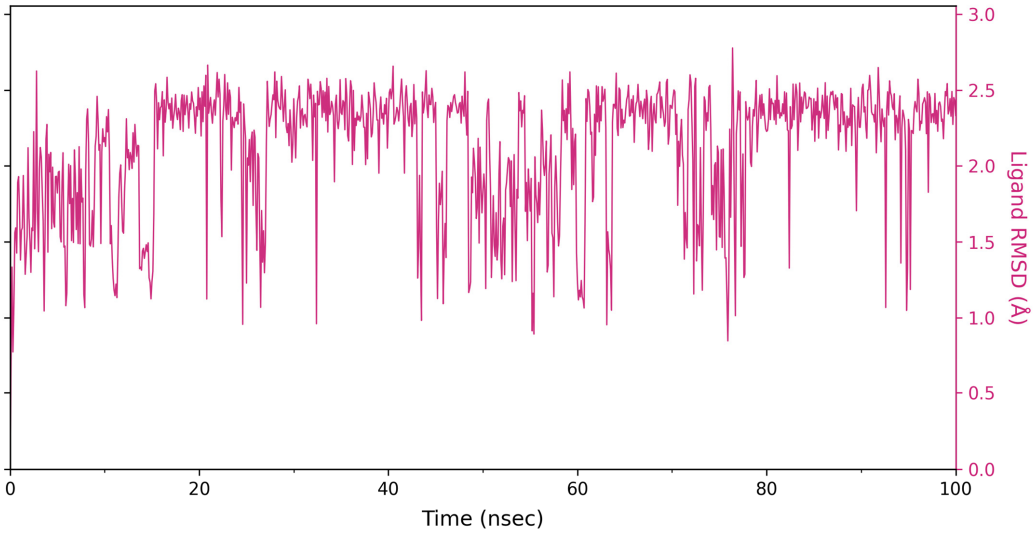


Figure 18. Molecular dynamics simulation (RMSD) of the interactions of MMs03492885_c1 within the PAK4 kinase.

2.5. TITIN Kinase

TITIN kinase (PDB:1TKI-A, OUT conformation) is auto-inhibited by its C-terminal tail, which wraps around the catalytic domain and obstructs the ATP binding site (Figure 19).

We targeted this C-terminal tail–activation segment interface for inhibitor design. Using PeptiDerive (Rosetta), a ten-amino acid peptide (VSVAKVKVAS) from the auto-inhibitory tail was identified as exhibiting the highest scoring profile (Figure 20).

The refinement of the complex interaction was carried out using FlexPepDock (https://flexpepdock.furmanlab.cs.huji.ac.il/, accessed on 24 June 2020). Rosetta.design 3.5 enabled us to modify three amino acids (S290L, K293M, S298Y) to improve this peptide's affinity. PIZSA (http://cospi.iiserpune.ac.in/pizsa/, accessed on 24 June 2020) allowed us to identify three adjacent peptide residues from the C-terminal auto-inhibitory tail (chain B) that contribute most significantly to the interaction with the kinase catalytic domain (chain A): Leu290 (side chain, backbone CO, and backbone NH), Met293 (side chain, backbone CO, and backbone NH), and Val294 (side chain, backbone CO, and backbone NH). The attempt to mimic this multiple peptide residue interaction through virtual screening using PyRx 0.8 resulted in compound MMs02074448 (Figure 21).

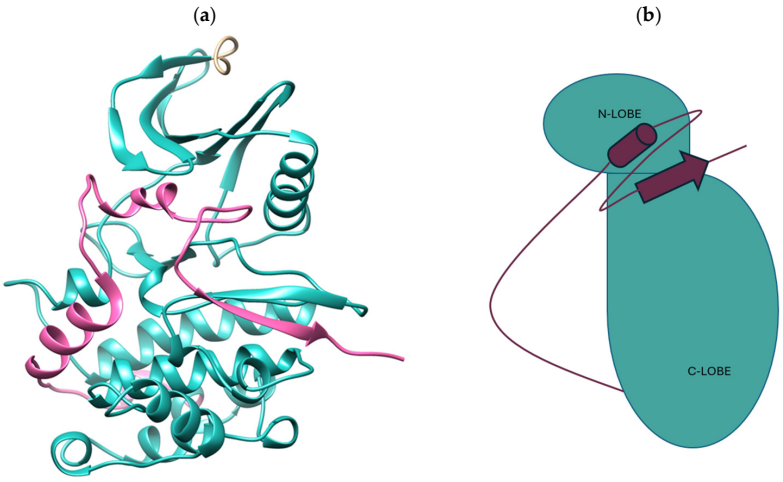


Figure 19. (**a**) X-ray crystal structure of the TITIN kinase (green), with the C-terminal auto-inhibitory tail highlighted in violet.(**b**) Schematic representation of the TITIN kinase. In (**a**,**b**), green represents the TITIN kinase, violet highlights the C-terminal auto-inhibitory tail, arrows indicate the beta sheet orientation, and cylinders represent α-helices in the ribbon representation of the C-terminal auto-inhibitory tail (violet).

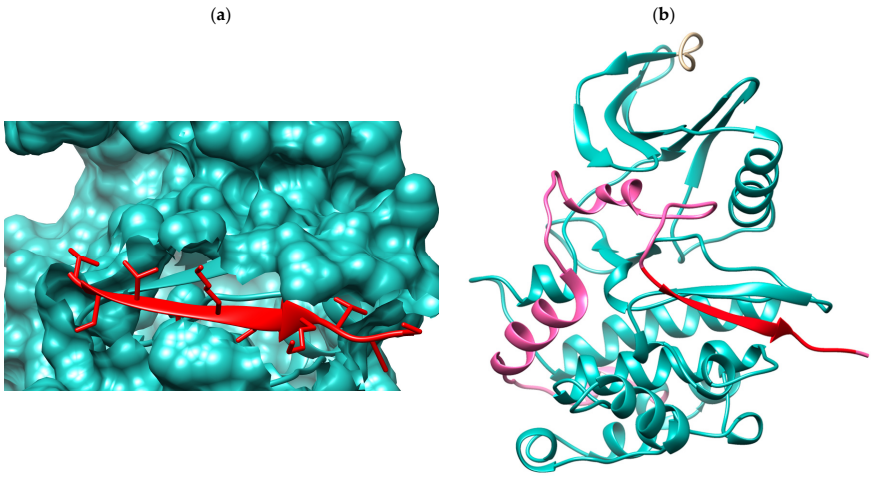


Figure 20. (**a**) Location of the ten-amino acid peptide (VSVAKVKVAS) from the C-terminal auto-inhibitory tail (in red) on the TITIN kinase surface (green); (**b**) Three-dimensional molecular structure visualization of this peptide (in red) in relation to the TITIN kinase (green). The red arrows indicate the beta sheet orientation of the C-terminal auto-inhibitory tail peptide within the binding pocket.

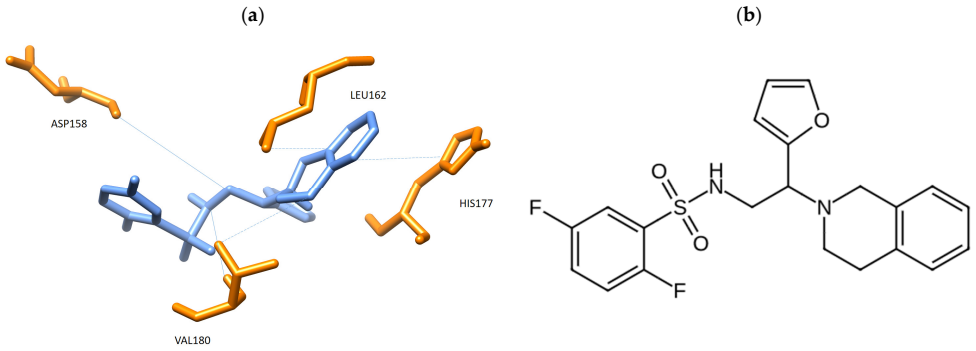


Figure 21. (**a**) Interactions involving the compound MMs02074448 within the TITIN kinase following docking, orange sticks represent kinase residues and blue sticks represent compound; (**b**) the 2D compound MMs02074448 obtained after virtual screening.

The docking analysis revealed the significance of hydrogen bonds between the compound and kinase residues (chain A) Asp158 and Val180, in addition to hydrophobic interactions with Leu162, His177, and Val180 (chain A) (Figure 21). Molecular dynamics simulations revealed ligand RMSD values plateauing around 2.6 Å (Figure 22).

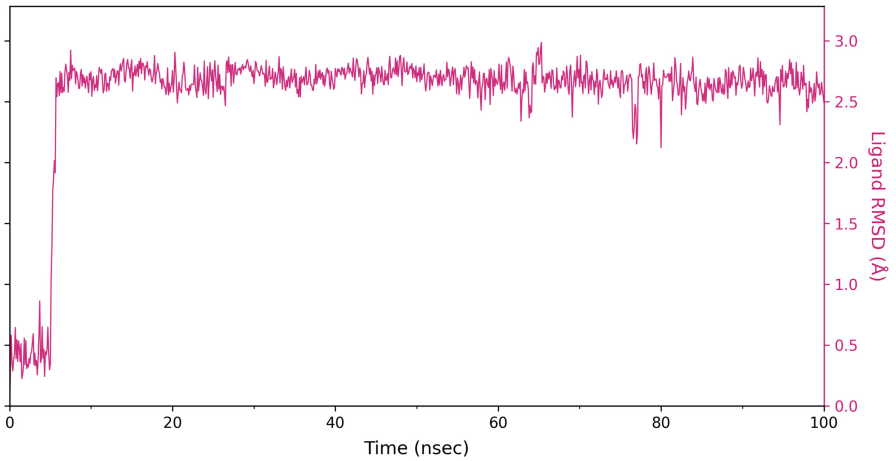


Figure 22. Molecular dynamics simulation (RMSD) of the interactions of MMs02074448 within the TITIN kinase.

To further elucidate the alternate binding mode suggested by the elevated RMSD plateau, a comparison was made between the initial docked pose and the equilibrated pose after 100 ns of molecular dynamics simulation using protein Cα-aligned superposition (Figure 23). The protein-aligned ligand RMSD between the two poses was 3.47 Å. PLIP interaction analysis within a 4.0 Å cutoff showed that all key docking contacts were maintained after equilibration, including the hydrogen-bond partner Val197 (2.73 Å) as well as hydrophobic contacts Leu179 (3.48 Å), His194 (2.91 Å), and Val197 (3.60 Å). The Asp175 contact distance increased from 2.71 to 3.21 Å but remained within the cutoff. Two new contacts were gained: a hydrogen bond with Asn176 (2.84 Å) and a hydrophobic interaction with Arg178 (3.57 Å, previously beyond cutoff at 4.53 Å), resulting in a consolidated interaction network. A representative superposition of the initial docked and equilibrated poses is shown in Figure 24.

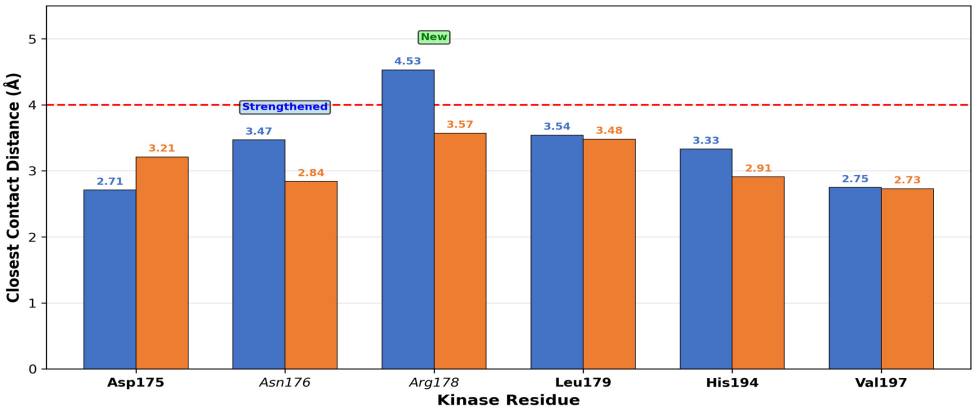


Figure 23. Contact distance comparison between initial docked and equilibrated (100 ns MD) poses of MMs02074448 within the TITIN kinase (ligand RMSD = 3.47 Å). Blue bars represent initial (docked) closest contact distances; orange bars represent equilibrated (100 ns) distances. The red dashed line indicates the 4.0 Å contact cutoff. Bold residue labels denote key contacts identified by docking (Figure 21); italic labels denote new contacts. All key docking contacts (Asp175, Leu179, His194, Val197) were maintained. Two new contacts were gained: Asn176 (H-bond) and Arg178 (hydrophobic).

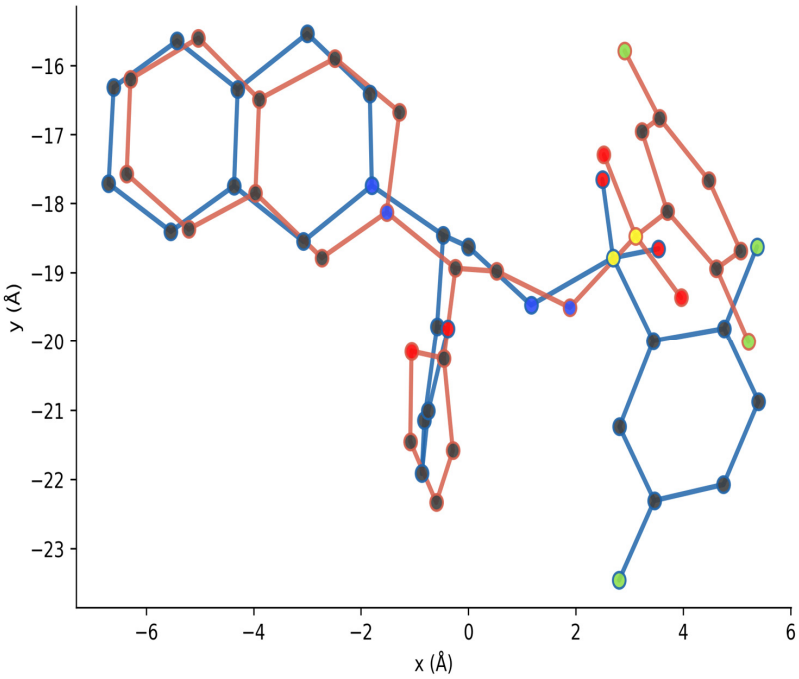


Figure 24. Cα-aligned superposition of the initial docked pose (blue) and the equilibrated pose after 100 ns MD (orange) of MMs02074448 within the TITIN kinase. Key binding-site residues are labeled. The displacement of the peripheral moiety is visible while the central scaffold remains anchored. Blue represents the initial docked pose; orange represents the equilibrated pose after 100 ns MD.

3. Discussion

We present a computational workflow integrating peptide design with ligand- and structure-based virtual screening to identify peptidomimetic kinase inhibitors. Applied across five kinases from distinct families (GSK3, PAK4, TTN, PKB and FLT3), the approach yielded one prioritized hit per target. Our findings reveal a clear relationship between activation segment conformation and peptidomimetic binding stability, with IN-state kinases showing more stable binding than OUT-state kinases. These results establish a framework for discovering selective kinase inhibitors through peptide-inspired design targeting activation segment interactions.

Molecular dynamics simulations revealed distinct stability patterns across the five kinases studied, providing valuable insights into the relationship between activation segment conformation and inhibitor binding stability. Systematic comparison of RMSD profiles demonstrates clear differences in binding stability that correlate with activation segment conformation, though with noteworthy exceptions.

FLT3, with its IN conformation of the activation segment, exhibited the most favorable stability profile with RMSD values consistently ranging between 1.5 and 2.0 Å and an average around 1.7–1.8 Å. This tight control of ligand conformation throughout the 100 ns simulation indicates highly stable interactions within the binding pocket formed by the folded activation segment. Similarly, PKB—also featuring an IN conformation—demonstrated good stability with RMSD values plateauing around 2.0 Å, placing it in the stable to moderately stable category according to our classification criteria.

In contrast, kinases with OUT conformations showed more variable stability profiles. GSK-3β, despite its OUT conformation, maintained relatively good stability with an average RMSD of 1.6 Å, though with significant periodic fluctuations between 1.2 and 2.1 Å, suggesting alternation between stable and less stable conformational states. PAK4 exhibited a broader range of RMSD values (1.5–2.4 Å), spanning our stable to moderately stable categories, while TTN demonstrated the least favorable profile with RMSD values

plateauing around 2.6 Å, placing it in the less stable category despite reaching a consistent equilibrium state.

The superior stability observed in IN conformation kinases (PKB and FLT3) can be attributed to several structural features. When in the IN conformation, the activation segment folds into the ATP binding site, creating a structured binding pocket that offers more consistent and well-defined interaction sites for inhibitors. This folded conformation provides a microenvironment with reduced conformational flexibility, allowing more stable hydrogen bonding networks and hydrophobic interactions to form between the inhibitor and the protein. Specifically, the binding pocket formed by the β6-β9 sheets or the entire A-loop pocket becomes more accessible and structurally defined in the IN conformation.

Conversely, kinases with OUT conformations (GSK-3β, PAK4, and TTN) present a more exposed and potentially more flexible binding environment. While this does not universally result in poor binding stability—as evidenced by GSK-3β's relatively good average RMSD—it does appear to correlate with greater conformational flexibility during molecular dynamics simulations. The exception observed with GSK-3β suggests that other factors beyond simply the IN/OUT classification, such as specific binding pocket characteristics, protein flexibility, and the nature of individual protein–ligand interactions, also significantly influence complex stability.

These findings provide important guidance for future inhibitor design efforts, suggesting that targeting kinases in their IN conformation may generally offer advantages for developing stable and effective inhibitors, though careful consideration of kinase-specific structural features remains essential for optimizing inhibitor design.

3.1. PKB Kinase: Binding Stability and Comparison with Existing Inhibitors

The PKB–MMs01663909 complex exhibited stable to moderately stable binding throughout the 100 ns simulation, with ligand RMSD values stabilizing around 2.0 Å. This stability indicates that the PH domain–activation segment interface provides a well-defined binding pocket in the IN conformation. These findings are consistent with and extend the work of Uhlenbrock et al. (2019) on covalent-allosteric Akt inhibitors, who similarly identified the inactive conformation as a promising target for selective inhibition [19]. While existing allosteric inhibitors such as MK-2206 [20] have demonstrated clinical efficacy, they face selectivity challenges due to structural similarities among AGC kinase family members. Our peptidomimetic approach exploits the specific PH domain–activation segment contacts (Phe309, Leu316, Asp323, Arg273), which are unique to PKB's auto-inhibited state, potentially offering improved selectivity over ATP-competitive strategies. This is consistent with observations by Lee et al. (2019) regarding the inherent selectivity advantages of peptide-based therapeutics [4].

3.2. FLT3 Kinase: JM Segment Targeting and Therapeutic Implications

The FLT3–MMs02451714 complex demonstrated the most favorable stability profile among all five kinases, with ligand RMSD values consistently between 1.5 and 2.0 Å (average 1.7–1.8 Å), placing it firmly in the stable category. This tight conformational control throughout the 100 ns simulation reflects the well-structured binding pocket formed by the folded JM segment–activation segment interface in the IN conformation. Our strategy represents a novel direction for FLT3 inhibition compared to current ATP-competitive inhibitors (Midostaurin, Gilteritinib), which face resistance challenges due to kinase domain mutations (D835Y, F691L). By exploiting the auto-inhibitory mechanism of the juxtamembrane segment originally described by Griffith et al. (2004) [18], our study is the first to translate this structural knowledge into a peptidomimetic inhibitor design strategy. The multiple hydrogen bonds observed with kinase residues Asp811, Arg810, Val808, Leu802,

Ser806, and Asp829 indicate that MMs02451714 successfully recapitulates the extensive contact network of the native JM segment, supporting the viability of this approach as an alternative to ATP-competitive inhibition.

3.3. GSK-3β Kinase: Pseudosubstrate Targeting and Conformational Dynamics

GSK-3β presents a particularly instructive case. Despite the OUT conformation, the MMs03699561 complex achieved a relatively low average RMSD of 1.6 Å, though with periodic oscillations between 1.2 and 2.1 Å, suggesting alternation between multiple binding modes. This dynamic behavior likely reflects the inherent flexibility of the exposed OUT-conformation binding site, where the P + 1 segment and substrate-binding groove lack the structural constraints imposed by a folded activation segment. Conventional ATP-competitive GSK-3β inhibitors such as Lithium and CHIR99021 show good efficacy but are associated with significant toxicity [26] 8 our peptidomimetic approach, by targeting the pS9 pseudosubstrate site rather than the ATP pocket, could potentially offer improved selectivity and reduced off-target effects. The S367Y modification introduced via Rosetta.design 3.5 extends beyond the structural characterization by Dajani et al. (2003) on the pS9 peptide–kinase interface [27], by demonstrating that computational optimization of the pseudosubstrate peptide can generate viable peptidomimetic scaffolds. Nonetheless, the pronounced RMSD oscillations indicate that further optimization—potentially through constrained analogs or cyclization—is needed to achieve more consistent binding stability.

3.4. PAK4 Kinase: PSD Targeting and Allosteric Inhibition

The PAK4–MMs03492885_c1 complex exhibited RMSD values ranging from 1.5 to 2.4 Å, spanning the stable to moderately stable categories, with a broader fluctuation range than the IN-conformation kinases. This behavior is consistent with the more exposed binding environment of the OUT-conformation substrate-binding site. Compared to existing PAK4 inhibitors such as PF-3758309 [21], which target the ATP binding site but face bioavailability limitations, our strategy of targeting the pseudosubstrate domain (PSD)–activation segment interface represents an unexplored inhibition mechanism. The identification of hydrogen bonds with Gly447 and Lys442, complemented by hydrophobic contact with Phe461, suggests that MMs03492885_c1 partially recapitulates the PSD–kinase contacts, though the conformational variability indicates room for structural optimization. These results complement the work of Won et al. (2019) on the PAK4–CREB axis, while offering a new perspective on allosteric inhibition mechanisms [21].

3.5. TITIN Kinase: C-Terminal Tail Inhibition and Structural Flexibility

TTN kinase represents the most challenging target in our study, with ligand RMSD values plateauing around 2.6 Å—the highest among the five kinases. Despite reaching a consistent equilibrium state, this elevated RMSD reflects the inherent structural flexibility of Titin kinase, which serves primarily a mechanosensing function rather than canonical signaling. The extended C-terminal tail–activation segment interface provides a relatively exposed binding surface in the OUT conformation, offering fewer structural constraints for stable ligand binding compared to the enclosed pockets of IN-conformation kinases. Literature on Titin kinase inhibition remains limited, as characterized in the literature, where the auto-inhibition mechanism via the C-terminal tail was described but not explored as a drug target. Our study is thus the first to apply a peptidomimetic strategy to this mechanism. The hydrogen bonds with Asp175 and Val197, combined with hydrophobic interactions involving Leu179, His194, and Val197, indicate that MMs02074448 engages a substantial portion of the C-terminal tail binding surface. PLIP analysis of the equilibrated structure confirmed that all key docking contacts were maintained after 100 ns, with Val197 preserving both its hydrogen bond (2.73 Å) and hydrophobic character, while Leu179 (3.48 Å) and His194

(2.91 Å) retained stable hydrophobic contacts. Two new interactions emerged: a hydrogen bond with Asn176 (2.84 Å) and a hydrophobic contact with Arg178 (3.57 Å), indicating that the ligand repositioning led to a consolidated rather than diminished interaction network. However, the elevated RMSD suggests that conformational restraint strategies—such as macrocyclization or introduction of non-natural amino acid mimetics—would be necessary to improve binding stability for therapeutic development [28].

Comparative analysis of RMSD profiles across the studied kinases reveals distinct stability patterns when applying our uniform classification criteria. FLT3 (IN conformation) demonstrates stable binding (RMSD 1.5–2.0 Å), while PKB (also IN conformation) shows stable to moderately stable behavior (RMSD ~2.0 Å). Among the OUT conformation kinases, GSK-3β maintains stability (RMSD ~1.6 Å) despite periodic fluctuations, and PAK4 spans stable to moderately stable classifications (RMSD 1.5–2.4 Å) with a wider fluctuation range. TTN (OUT conformation) falls into the less stable category (RMSD ~2.6 Å), though it maintains a consistent equilibrium state. These results demonstrate that while activation segment conformation influences binding stability, other factors, including specific binding pocket characteristics and individual protein–ligand interactions, also significantly impact complex stability.

Taken together, the superior stability profiles of both FLT3 and PKB provide strong evidence that the IN conformation of the activation segment creates a more favorable context for peptidomimetic inhibitor binding.

These findings suggest that targeting kinases in their IN conformation might be a more promising strategy for inhibitor design, as evidenced by the significantly more stable binding profiles observed. The contrast between the highly stable RMSD profiles of IN conformation kinases (particularly FLT3's 1.5–2.0 Å range) and the more variable profiles of OUT conformation kinases provides a clear direction for future inhibitor development efforts.

These findings are consistent with and extend previous structural studies on kinase regulation. Reference [15] described the fundamental role of activation segment conformation in controlling kinase activity, and our results demonstrate that this conformational distinction also carries practical implications for inhibitor design. For PKB, our peptidomimetic approach targeting the PH domain–activation segment interface provides an alternative to existing allosteric inhibitors such as MK-2206, potentially offering improved selectivity by exploiting natural regulatory interactions rather than the conserved ATP-binding site. For FLT3, our strategy of targeting the juxtamembrane auto-inhibitory mechanism represents a novel direction compared to current ATP-competitive inhibitors like Midostaurin and Gilteritinib, which face resistance challenges due to kinase domain mutations.

Several aspects of this work represent novel contributions. First, this is the first systematic comparison of peptidomimetic inhibitor binding stability across kinases with different activation segment conformations. Second, the targeting of the pseudosubstrate domain in PAK4 and the C-terminal auto-inhibitory tail in TTN for peptidomimetic design has not been previously reported. Third, our integrated workflow combining PeptiDerive (Rosetta), RosettaDesign version 3.5, pharmacophore modeling, and molecular dynamics validation provides a reproducible framework for future peptidomimetic inhibitor discovery.

Several limitations should be acknowledged. The computational predictions require experimental validation through binding assays, enzymatic inhibition studies, and cell-based assays. The use of the MMsINC (http://mms.dsfarm.unipd.it/MMsINC/search/, accessed on 7 July 2022) library, while enriched for peptidomimetic scaffolds, provides more limited chemical diversity compared to ultra-large libraries such as Enamine REAL or ZINC. Additionally, the 100 ns simulation timescale, while sufficient to assess initial binding stability, may not capture slower conformational transitions that could affect long-term inhibitor efficacy.

Future research should prioritize experimental validation of the most promising compounds, particularly MMs01663909 (PKB) and MMs02451714 (FLT3), which demonstrated the most stable binding profiles. Further optimization of inhibitors for GSK-3β, PAK4, and TTN should focus on enhancing binding stability through structure-guided modifications. Screening of larger chemical libraries against the identified pharmacophore models could expand the chemical diversity of candidate inhibitors. Finally, extending this approach to additional kinases with known regulatory terminal tail interactions could broaden the applicability of activation segment-targeted peptidomimetic inhibition as a therapeutic strategy.

4. Materials and Methods

Computational Workflow Overview: Our peptidomimetic kinase inhibitor design pipeline consists of five integrated steps (Figure 25): (1) structure preparation and activation segment classification, (2) peptide design and optimization, (3) peptidomimetic enumeration, (4) virtual screening and molecular docking, and (5) molecular dynamics validation. This workflow was applied uniformly across five kinase targets from distinct families.

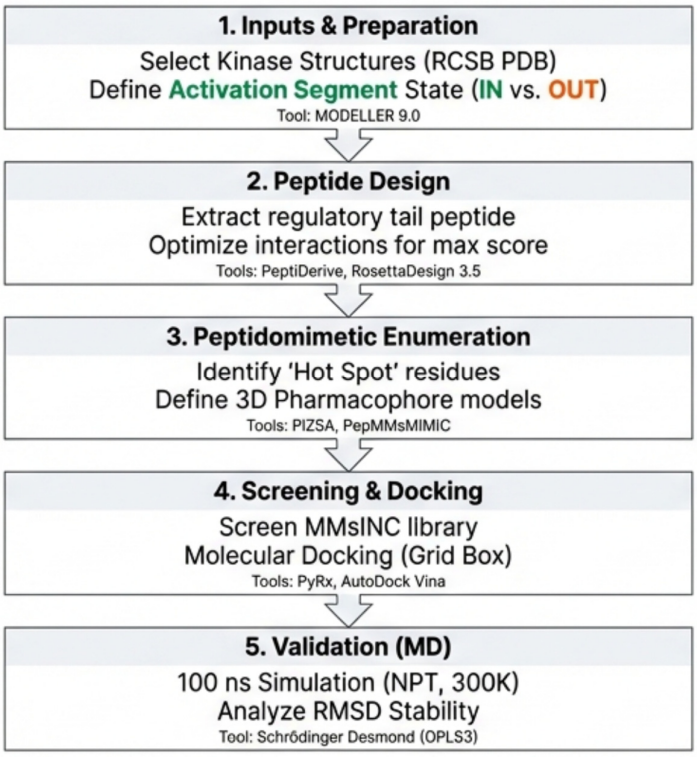


Figure 25. Five-step computational workflow for peptidomimetic kinase inhibitor design.

4.1. Data Collection and Preparation

The three-dimensional structures of kinases were obtained from the RCSB Protein Data Bank. We specifically selected kinases that exhibited direct peptide interactions between the terminal tail peptide chain and the activation segment, in either its open (DFG in) or closed (DFG out) configuration. The unresolved regions of the catalytic domains in the selected structures were subsequently modeled using MODELLER version 9.0 [29].

4.2. Peptidomimetics

Phase 1: Selecting the optimal region of the peptide chain, which encompasses the most effective binding elements within the activation segment cleft, involved the following steps:

Selection of the most favorable peptide region for efficient interaction with the activation segment and optimization of interactions within this region using PeptiDerive (Rosetta) software [30], which employs a protocol for the selection and evaluation of protein–peptide interface peptides.

Enhancement of peptide-activation segment interactions by maximizing the interaction score using RosettaDesign version 3.5 software [31]. Fragments contributing significantly to binding energy were considered as candidates to compete with existing interactions [30]. The Rosetta Cluster application incorporated the top 500 performing models, with peptide backbone atoms not exceeding a RMSD of 2 Å [32].

Following the design of the optimal peptide sequence, the resulting complex structure was minimized. Re-optimization of peptide–kinase interactions was performed using Rosetta FlexPepDock (https://flexpepdock.furmanlab.cs.huji.ac.il/, accessed on 24 June 2020), which is capable of refining peptide-protein complex structures [14].

Finally, the evaluation and ranking of the resulting designed sequences were conducted [31].

Phase 2: Optimizing peptide fragments that showed improved interaction scores to develop kinase inhibition ligands involved the following sequence of steps:

PIZSA (http://cospi.iiserpune.ac.in/pizsa/, accessed on 24 June 2020) software identified peptide residues with the highest binding contribution scores for mimetic design [33].

PepMMsMIMIC (http://mms.dsfarm.unipd.it/pepMMsMIMIC/, accessed on 7 July 2022) software [34] translated key residue interactions into 3D pharmacophore models, capturing essential binding features.

Pharmacophore models screened against the MMsINC (http://mms.dsfarm.unipd.it/MMsINC/search/, accessed on 7 July 2022) compound library using PyRx 0.8 to identify molecules with structural similarity to binding motifs [35]. The MMsINC library was selected for virtual screening based on its focus on peptidomimetic scaffolds that mimic peptide secondary structures (β-turns, α-helices, extended conformations). Unlike general screening libraries (Enamine REAL, Mcule, ZINC) optimized for small-molecule drug-likeness, MMsINC contains approximately 150,000 compounds enriched in constrained amino acid analogs and cyclic peptides relevant to our peptide-inspired design strategy. Additionally, MMsINC compounds are annotated with synthetic accessibility information, facilitating experimental follow-up. This focused approach prioritizes peptide-relevant chemical space over absolute compound numbers.

AutoDock Vina 1.1.2 [36] performed docking simulations using gradient-based optimization within minimized grid boxes centered on activation segment binding sites.

Best-scoring compounds underwent re-docking to optimize positioning and interactions within target binding pockets.

This approach identified small molecules capable of mimicking critical peptide-protein interactions while maintaining drug-like properties.

4.3. Dynamic Study

Protein–ligand complex stability was evaluated using Schrödinger's Desmond v6.6 software (Schrödinger Suite 2016, Multisim v3.8.5.19) with the OPLS3 force field. Systems were prepared by adding hydrogen atoms, placing ions in experimental positions, and reconstructing missing residues. Each complex was solvated in a TIP3P water box with a 10 Å buffer, and neutralized with Na^+ ions [37]. A two-phase equilibration protocol was employed: (1) energy minimization to 25 kcal/mol/Å gradient threshold, and (2) 100 ps NPT equilibration with temperature annealing from 0 K to 300 K. Production simulations ran for 100 ns in the NPT ensemble (1.01325 bar, 300 K) using the Martyna–Tobias–Klein barostat (τ = 2.0 ps) and Nose–Hoover thermostat (τ = 1.0 ps). A 2 fs timestep was used

with RESPA integration, and a 9.0 Å cutoff for non-bonded interactions. Trajectory frames were saved every 100 ps. Analysis focused on RMSD calculations of ligand heavy atoms and protein Cα atoms, using the initial docked structure as reference [37].

Ligand RMSD was calculated using all heavy atoms of the peptidomimetic, aligned to the initial docked pose, to assess binding mode stability throughout the 100 ns MD trajectories. LIGAND RMSD values were computed at 100 ps intervals.

The limitations of this computational approach and future research directions are discussed in the Section 3.

5. Conclusions

This study has provided a deeper insight into the computational design of peptidomimetic compounds that mimic regulatory terminal tail interactions with the activation segment of kinases. By examining five kinases from different families (GSK3, PAK4, TTN, PKB, and FLT3), we have demonstrated how these interactions can be exploited for selective inhibitor design.

Our results revealed complex stability patterns that do not uniformly correlate with activation segment conformations. While FLT3 (IN conformation) demonstrated excellent stability with LIGAND RMSD values between 1.5 and 2.0 Å, we observed that GSK-3β (OUT conformation) showed comparable or better stability with an average LIGAND RMSD of 1.6 Å, though with some conformational fluctuations. PKB (IN conformation) maintained consistent LIGAND RMSD values around 2.0 Å, while PAK4 (OUT conformation) exhibited a partially overlapping stability range (1.5–2.4 Å), indicating that factors beyond just conformation type influence binding stability. TTN (OUT conformation) stabilized at a higher LIGAND RMSD plateau (2.6 Å), likely reflecting its structural role and inherent flexibility.

These findings suggest that selective kinase inhibition through activation segment targeting requires consideration of multiple factors: (1) the specific binding pocket characteristics of individual kinases, (2) the nature and strength of key protein–ligand interactions, and (3) the conformational dynamics of the activation segment. The designed peptidomimetic compounds demonstrated promising computational stability and interaction profiles, particularly for FLT3 and PKB, though further optimization is needed to enhance stability for GSK-3β, PAK4, and TTN. It should be emphasized that these computational predictions require experimental validation through binding assays, enzymatic inhibition studies, and cell-based assays to confirm the actual inhibitory potential of these compounds. The GSK-3β system exemplifies the importance of analyzing complete LIGAND RMSD profiles rather than relying solely on average values, as significant fluctuations can indicate dynamic binding behavior that might affect inhibitor efficacy.

The approach presented here opens new avenues for the development of selective kinase inhibitors by exploiting natural regulatory mechanisms. Further research should be undertaken to experimentally validate these computational predictions through binding assays, enzymatic inhibition studies, and cell-based assays. A further study could assess the pharmacokinetic properties of these compounds and conduct expanded cross-docking studies to establish a more comprehensive selectivity profile. This approach may offer significant advantages over traditional ATP-competitive inhibitors, particularly for kinases where selectivity has been challenging to achieve.

Author Contributions: Designing research studies: A.A. (Adil Ahiri) and A.A. (Aziz Aboulmouhajir); conducting experiments: A.A. (Adil Ahiri); analyzing data: A.A. (Adil Ahiri) and A.A. (Aziz Aboulmouhajir); writing the manuscript: A.A. (Adil Ahiri) and A.A. (Aziz Aboulmouhajir); final approval of this manuscript: A.A. (Adil Ahiri) and A.A. (Aziz Aboulmouhajir). All authors have read and agreed to the published version of the manuscript.

Funding: This research received no external funding.

Institutional Review Board Statement: Not applicable.

Informed Consent Statement: Not applicable.

Data Availability Statement: The data presented in this study are available in RCSB PDB at https://www.rcsb.org/ (accessed on 15 January 2020).

Conflicts of Interest: The authors declare no conflicts of interest.

Abbreviations

The following abbreviations are used in this manuscript:

ATP	Adenosine Triphosphate
GSK-3β	Glycogen Synthase Kinase 3β
PAK4	p21-activated Kinase 4
TTN	Titin Kinase
PKB	Protein Kinase B
FLT3	FMS-like Tyrosine Kinase 3
PH	Pleckstrin Homology
PI3K	Phosphatidylinositide-3-kinase
JM	Juxtamembrane
TM	Transmembrane
PBD	p21-binding Domain
PSD	Pseudosubstrate Domain
LIGAND RMSD	Root Mean Square Deviation

References

1. Wu, P.; Nielsen, T.E.; Clausen, M.H. Small-Molecule Kinase Inhibitors: An Analysis of FDA-Approved Drugs. *Drug Discov. Today* **2016**, *21*, 5–10. [CrossRef] [PubMed]
2. Bain, J.; Plater, L.; Elliott, M.; Shpiro, N.; Hastie, C.J.; Mclauchlan, H.; Klevernic, I.; Arthur, J.S.C.; Alessi, D.R.; Cohen, P. The Selectivity of Protein Kinase Inhibitors: A Further Update. *Biochem. J.* **2007**, *408*, 297–315. [CrossRef] [PubMed]
3. Krim Gavrin, L.; Saiah, E. Approaches to Discover Non-ATP Site Kinase Inhibitors. *MedChemComm* **2013**, *4*, 41–51. [CrossRef]
4. Lee, A.C.-L.; Harris, J.L.; Khanna, K.K.; Hong, J.-H. A Comprehensive Review on Current Advances in Peptide Drug Development and Design. *Int. J. Mol. Sci.* **2019**, *20*, 2383. [CrossRef]
5. Wu, P.; Nielsen, T.E.; Clausen, M.H. FDA-Approved Small-Molecule Kinase Inhibitors. *Trends Pharmacol. Sci.* **2015**, *36*, 422–439. [CrossRef]
6. Biswas, B.; Huang, Y.-H.; Craik, D.J.; Wang, C.K. The Prospect of Substrate-Based Kinase Inhibitors to Improve Target Selectivity and Overcome Drug Resistance. *Chem. Sci.* **2024**, *15*, 13130–13147. [CrossRef]
7. Wang, J.; Zheng, P.; Yu, J.; Yang, X.; Zhang, J. Rational Design of Small-Sized Peptidomimetic Inhibitors Disrupting Protein–Protein Interaction. *RSC Med. Chem.* **2024**, *15*, 2212–2225. [CrossRef]
8. Nada, H.; Choi, Y.; Kim, S.; Jeong, K.S.; Meanwell, N.A.; Lee, K. New Insights into Protein–Protein Interaction Modulators in Drug Discovery and Therapeutic Advance. *Signal Transduct. Target. Ther.* **2024**, *9*, 341. [CrossRef]
9. Qvit, N. Chapter 15—Therapeutic Peptides Targeting Protein Kinase: Progress, Challenges, and Future Directions, Featuring Cancer and Cardiovascular Disease. In *Peptide and Peptidomimetic Therapeutics*; Qvit, N., Rubin, S.J.S., Eds.; Academic Press: Cambridge, MA, USA, 2022; pp. 333–356. ISBN 978-0-12-820141-1.
10. Crunkhorn, S. Anticancer Drugs: Stapled Peptide Reactivates P53. *Nat. Rev. Drug Discov.* **2013**, *12*, 741. [CrossRef]
11. Watt, P.M. Screening for Peptide Drugs from the Natural Repertoire of Biodiverse Protein Folds. *Nat. Biotechnol.* **2006**, *24*, 177. [CrossRef]
12. Alam, K.A. Studies on Selectivity Determinants of Protein Kinase Inhibitor Binding. Ph.D. Thesis, University of Bergen, Bergen, Norway, 2017.
13. Clackson, T.; Wells, J.A. A Hot Spot of Binding Energy in a Hormone-Receptor Interface. *Science* **1995**, *267*, 383–386. [CrossRef]
14. London, N.; Raveh, B.; Cohen, E.; Fathi, G.; Schueler-Furman, O. Rosetta FlexPepDock Web Server—High Resolution Modeling of Peptide–Protein Interactions. *Nucleic Acids Res.* **2011**, *39*, W249–W253. [CrossRef] [PubMed]

15. Nolen, B.; Taylor, S.; Ghosh, G. Regulation of Protein Kinases: Controlling Activity through Activation Segment Conformation. *Mol. Cell* **2004**, *15*, 661–675. [CrossRef] [PubMed]
16. Pflug, A.; Schimpl, M.; Nissink, J.W.M.; Overman, R.C.; Rawlins, P.B.; Truman, C.; Underwood, E.; Warwicker, J.; Winter-Holt, J.; McCoull, W. A-Loop Interactions in Mer Tyrosine Kinase Give Rise to Inhibitors with Two-Step Mechanism and Long Residence Time of Binding. *Biochem. J.* **2020**, *477*, 4443–4452. [CrossRef] [PubMed]
17. Kannan, N.; Haste, N.; Taylor, S.S.; Neuwald, A.F. The Hallmark of AGC Kinase Functional Divergence Is Its C-Terminal Tail, a Cis-Acting Regulatory Module. *Proc. Natl. Acad. Sci. USA* **2007**, *104*, 1272–1277, Correction in *Proc. Natl. Acad. Sci. USA* **2008**, *105*, 9130. https://doi.org/10.1073/pnas.0804708105. [CrossRef]
18. Griffith, J.; Black, J.; Faerman, C.; Swenson, L.; Wynn, M.; Lu, F.; Lippke, J.; Saxena, K. The Structural Basis for Autoinhibition of FLT3 by the Juxtamembrane Domain. *Mol. Cell* **2004**, *13*, 169–178. [CrossRef]
19. Uhlenbrock, N.; Smith, S.; Weisner, J.; Landel, I.; Lindemann, M.; Le, T.A.; Hardick, J.; Gontla, R.; Scheinpflug, R.; Czodrowski, P.; et al. Structural and Chemical Insights into the Covalent-Allosteric Inhibition of the Protein Kinase Akt. *Chem. Sci.* **2019**, *10*, 3573–3585. [CrossRef]
20. Nussinov, R.; Tsai, C.-J.; Jang, H. Autoinhibition Can Identify Rare Driver Mutations and Advise Pharmacology. *FASEB J.* **2020**, *34*, 16–29. [CrossRef]
21. Won, S.-Y.; Park, J.-J.; Shin, E.-Y.; Kim, E.-G. PAK4 Signaling in Health and Disease: Defining the PAK4–CREB Axis. *Exp. Mol. Med.* **2019**, *51*, 1–9. [CrossRef]
22. Schwarz, D.; Merget, B.; Deane, C.; Fulle, S. Modeling Conformational Flexibility of Kinases in Inactive States. *Proteins Struct. Funct. Bioinform.* **2019**, *87*, 943–951. [CrossRef]
23. Ahiri, A.; Garmes, H.; Podlipnik, C.; Aboulmouhajir, A. Insights into Evolutionary Interaction Patterns of the "Phosphorylation Activation Segment" in Kinase. *Bioinformation* **2019**, *15*, 666–677. [CrossRef]
24. Endicott, J.A.; Noble, M.E.M.; Johnson, L.N. The Structural Basis for Control of Eukaryotic Protein Kinases. *Annu. Rev. Biochem.* **2012**, *81*, 587–613. [CrossRef]
25. Jenardhanan, P.; Panneerselvam, M.; Mathur, P.P. Targeting Kinase Interaction Networks: A New Paradigm in PPI Based Design of Kinase Inhibitors. *Curr. Top. Med. Chem.* **2019**, *19*, 467–485. [CrossRef]
26. Beurel, E.; Grieco, S.F.; Jope, R.S. Glycogen Synthase Kinase-3 (GSK3): Regulation, Actions, and Diseases. *Pharmacol. Ther.* **2015**, *148*, 114–131. [CrossRef]
27. Dajani, R.; Fraser, E.; Roe, S.M.; Yeo, M.; Good, V.M.; Thompson, V.; Dale, T.C.; Pearl, L.H. Structural Basis for Recruitment of Glycogen Synthase Kinase 3β to the Axin—APC Scaffold Complex. *EMBO J.* **2003**, *22*, 494–501. [CrossRef] [PubMed]
28. Gautel, M. Cytoskeletal Protein Kinases: Titin and Its Relations in Mechanosensing. *Pflug. Arch.* **2011**, *462*, 119–134. [CrossRef] [PubMed]
29. Webb, B.; Sali, A. Comparative Protein Structure Modeling Using MODELLER. *Curr. Protoc. Bioinform.* **2014**, *47*, 5–6. [CrossRef] [PubMed]
30. Sedan, Y.; Marcu, O.; Lyskov, S.; Schueler-Furman, O. Peptiderive Server: Derive Peptide Inhibitors from Protein–Protein Interactions. *Nucleic Acids Res.* **2016**, *44*, W536–W541. [CrossRef]
31. Liu, Y.; Kuhlman, B. RosettaDesign Server for Protein Design. *Nucleic Acids Res.* **2006**, *34*, W235–W238. [CrossRef]
32. Gray, J.J.; Moughon, S.; Wang, C.; Schueler-Furman, O.; Kuhlman, B.; Rohl, C.A.; Baker, D. Protein–Protein Docking with Simultaneous Optimization of Rigid-Body Displacement and Side-Chain Conformations. *J. Mol. Biol.* **2003**, *331*, 281–299. [CrossRef]
33. Roy, A.A.; Dhawanjewar, A.S.; Sharma, P.; Singh, G.; Madhusudhan, M.S. Protein Interaction Z Score Assessment (PIZSA): An Empirical Scoring Scheme for Evaluation of Protein–Protein Interactions. *Nucleic Acids Res.* **2019**, *47*, W331–W337. [CrossRef]
34. Floris, M.; Masciocchi, J.; Fanton, M.; Moro, S. Swimming into Peptidomimetic Chemical Space Using pepMMsMIMIC. *Nucleic Acids Res.* **2011**, *39*, W261–W269. [CrossRef]
35. Masciocchi, J.; Frau, G.; Fanton, M.; Sturlese, M.; Floris, M.; Pireddu, L.; Palla, P.; Cedrati, F.; Rodriguez-Tomé, P.; Moro, S. MMsINC: A Large-Scale Chemoinformatics Database. *Nucleic Acids Res.* **2009**, *37*, D284–D290. [CrossRef]
36. Trott, O.; Olson, A.J. AutoDock Vina: Improving the Speed and Accuracy of Docking with a New Scoring Function, Efficient Optimization, and Multithreading. *J. Comput. Chem.* **2010**, *31*, 455–461. [CrossRef]
37. Schrödinger, L. *Schrödinger Suite*; Schrödinger LLC: New York, NY, USA, 2016.

Disclaimer/Publisher's Note: The statements, opinions and data contained in all publications are solely those of the individual author(s) and contributor(s) and not of MDPI and/or the editor(s). MDPI and/or the editor(s) disclaim responsibility for any injury to people or property resulting from any ideas, methods, instructions or products referred to in the content.